Title
Coupling of Nitrous Oxide and Methane by Global Atmospheric Chemistry

Journal
Science, 330(6006)

ISSN
0036-8075

Authors
Prather, Michael J
Hsu, Juno

Publication Date
2010-11-12

DOI
10.1126/science.1196285

Coupling of Nitrous Oxide and Methane by Global Atmospheric Chemistry

Michael J. Prather and Juno Hsu

Nitrous oxide (N_2O) and methane (CH_4) are chemically reactive greenhouse gases with well-documented atmospheric concentration increases that are attributable to anthropogenic activities. We quantified the link between N_2O and CH_4 emissions through the coupled chemistries of the stratosphere and troposphere. Specifically, we simulated the coupled perturbations of increased N_2O abundance, leading to stratospheric ozone (O_3) depletion, altered solar ultraviolet radiation, altered stratosphere-to-troposphere O_3 flux, increased tropospheric hydroxyl radical concentration, and finally lower concentrations of CH_4. The ratio of CH_4 per N_2O change, −36% by mole fraction, offsets a fraction of the greenhouse effect attributable to N_2O emissions. These CH_4 decreases are tied to the 108-year chemical mode of N_2O, which is nine times longer than the residence time of direct CH_4 emissions.

Methane (CH_4) has environmental impacts beyond those of a direct greenhouse gas, through atmospheric chemistry that enhances the abundance of tropospheric ozone (O_3) and decreases that of hydroxyl radicals (OH) and hence the atmospheric lifetime of many other pollutants (*1*, *2*). Likewise, nitrous oxide (N_2O) is a known O_3-depleting substance (*3*, *4*). Both CH_4 and N_2O interact directly in the chemistry of stratospheric O_3, where global CH_4 concentration increases drive proportional but much smaller N_2O increases (*5*). The pathway of how N_2O affects global CH_4 is more complex, involving the coupling of stratospheric O_3 depletion with global tropospheric chemistry through OH, and consequently the lifetime of CH_4.

This chemical coupling of the stratosphere and troposphere alters one's expectations about the amplitude and persistence of anthropogenic perturbations. Here we describe four multidecade numerical simulation experiments—one control and three perturbations runs—which have been designed to find such coupling between N_2O and CH_4 through analysis of long-lived chemical modes. We define modes as the perturbation patterns in the abundances of all chemical species resulting from, for example, the addition of one species (i.e., eigenvectors of the linearized system). In atmospheric chemistry, the most important modes are the long-lived, slowly decaying ones associated with N_2O and CH_4, because these have the largest environmental impacts.

The University of California Irvine's three-dimensional chemistry-transport model incorporates algorithms for both stratospheric and tropospheric chemistry (*5*–*7*). The meteorology and trace gas emissions in this study are representative of conditions in the year 2005 (*7*). For our control run, the CH_4 and N_2O emissions are prescribed to achieve steady-state abundances of 1775 and 320 parts per billion (ppb), respectively. The annual budgets for N_2O, CH_4, and carbon monoxide (CO) from year 80 of this run are summarized in Table 1. Surface N_2O emissions of 13 Tg of N/year are matched by stratospheric loss. There are small terms (~1%) in the budget accounting for stratospheric production ($N + NO_2$) and tropospheric loss [$O(^1D) + N_2O$]. The budget lifetime of N_2O is 118 years. Surface CH_4 emissions of 643 Tg/year are balanced by tropospheric (95%) and stratospheric (5%) loss, giving a budget lifetime of 7.8 years, which is within the range of models reported in (*8*) (Table 1). Surface CO emissions of 1050 Tg/year are augmented by 2070 Tg/year from photochemical production in the atmosphere.

The chemical modes, using an annually repeating meteorology, are five-dimensional (species, time of year, and three spatial dimensions) quantities, as shown in previous studies (*5*, *9*, *10*). Here we focus on the global burden on 1 January, thus ignoring the spatial and seasonal variations shown in (*9*). Modes are calculated from the difference between a perturbation and the control simulation. The same initialization and 80-year control simulation (C1) is used in all cases. The N_2O perturbation (simulation C2) introduces a pulse of 10 Tg of N from N_2O in the lowest four model layers on top of the initial conditions; the CO perturbation (simulation C3) introduces 100 Tg of CO; and the CH_4 perturbation (simulation C4) introduces 10 Tg of CH_4. In the perturbation-minus-control differences, the shorter-lived modes (those associated with other chemical species, interhemispheric mixing, and stratosphere-troposphere exchange) decay within a few years, leaving behind a combination of the N_2O-driven mode 1 (108 years) and the CH_4-driven mode 2 (12.5 years).

The pulse of N_2O alone (C2 – C1) induces perturbations in almost all species as shown in Fig. 1A. The relative perturbations in total atmospheric burden (in kilograms) eventually lock into the pattern of the 108-year mode 1: positive perturbations (solid lines) for N_2O, odd nitrogen species (NOy), and upper tropospheric O_3; and negative (dashed lines) for CH_4, CO, total O_3, and lower tropospheric O_3. The relative amplitudes, in terms of percent of the steady-state control C1, are shown in Fig. 2. For the long-lived gases N_2O and CH_4, these have only slight variations with altitude, but for O_3, the pattern changes sign and varies greatly with latitude.

The CO pulse (C3 – C1) is shown in Fig. 1B. Results are plotted beginning 1 year after the pulse, when the initial 10^{11} kg of CO and its related perturbation of tropospheric O_3 have mostly decayed. The CH_4 perturbation, caused by the CO-driven decrease in OH, is established by year 1 and decays with the mode 2 time of 12.5 years, which is longer than the budget lifetime of 7.8 years. Perturbations of CO and total O_3 also occur in mode 2 and are apparent for at least the first 60 years. The N_2O perturbation is predominantly in mode 1 and is caused by increased CH_4 in the stratosphere [see the stratospheric chemistry modes in (*5*)]. Following the chemical perturbations by the difference between two runs, C3 – C1, becomes difficult when the amplitudes in modes 1 and 2 become comparable as they do near the end of the simulation in Fig. 1B. The control C1 does not begin in an exact steady state and thus has a drift that is also a combination of the two modes, with the transition in O_3 and CO amplitudes from 2 to 1 occurring near year 50. This interference of the modes causes the derived amplitudes of CO and O_3 to diverge from a simple decay curve (e-fold), plus some noise in the subtraction (thin lines in Fig. 1B). This transition does not affect Fig. 1A, where the amplitudes in the longer-lived mode 1 are much larger.

In these perturbations, modes 1 and 2 can be separated and then traced back to a value at time zero, knowing that exponential decay is fixed globally for each mode. These time-zero amplitudes are reported in Table 2 for the three perturbations and the primary species of interest here (N_2O, NOy, CH_4, total O_3, and tropospheric O_3). Chemical modes, like eigenvectors, are scalable patterns; and thus in Table 2, mode 1 perturbations can be characterized by the total mass of N_2O, and mode 2 perturbations by that of CH_4. The pulse of 10 Tg of N from N_2O (C2) leads to a mode 1 amplitude of 10.2 Tg of N. Loss of this surface pulse is minimal in the first year as it mixes slowly into the region of stratospheric

Table 1. Annual mean chemical budget terms (in teragrams/year) and budget lifetimes. Surface emissions, production (prod), and loss are in teragrams/year except for N_2O, which are in teragrams of N/year. Terms are split into stratosphere (strat) and troposphere (trop). CO surface deposition is included in trop loss. CH_4 surface deposition is not included, and it would have shortened the CH_4 lifetime to 7.44 years, which is still within the standard deviation of models in (*8*), 8.7 ± 1.3 years.

Species	Surface	Trop prod	Trop loss	Strat prod	Strat loss	Lifetime (years)
N_2O	+13.0	0	−0.14	+0.14	−13.1	118.3
CH_4	+643	0	−611	0	−32	7.8
CO	+1050	+2070	−2955	0	−165	0.33

Department of Earth System Science, University of California, Irvine, CA 92697–3100, USA.

destruction. Thus, the avoided loss, about 0.2 Tg of N, adds to the amplitude of mode 1, amplifying the integrated radiative forcing from the N_2O pulse. Such an increase of about 2% should be applied to all greenhouse gases with stratospheric loss, such as chlorofluorocarbons, but not to those with tropospheric loss, such as hydrofluorocarbons. In a similar but opposite vein, the pulse of 10 Tg of CH_4 (C4) has an amplitude of only 9.85 Tg in mode 2, because the most rapid loss occurs in the lower atmosphere where it is emitted. The N_2O pulse (C2) produces a CH_4 amplitude of –2.1 Tg in mode 1 and +2.8 Tg in mode 2. This pulse must also excite other, short-lived modes (not seen here) with a net CH_4 amplitude of –0.7 Tg, because the initial CH_4 perturbation is zero. The overall negative perturbation of CH_4 appears within the first year, and within two decades, the CH_4 perturbation parallels that of N_2O in mode 1.

This study looks at the coupled chemistry of stratosphere and troposphere, and thus we examine the mode patterns in Fig. 2 to trace causality, beginning with a surface increase in N_2O of 10% (32 ppb). The increase in N_2O directly causes an increase in NOy, which depletes O_3 by about 2% in the middle stratosphere (a height of 25 to 40 km). The decrease in O_3 allows greater penetration of solar ultraviolet (UV) into the middle stratosphere, enhancing the destruction of N_2O. Thus, the relative perturbation of N_2O declines from +10% to about +8.5% above 35 km. The relative increase in NOy is about the same as that in its source (N_2O) below 30 km, but rapidly falls off aloft where the quadratic photochemical loss of NOy buffers its abundance. The maximum decrease of –1.2% in the overhead O_3 column occurs at about 22 km and varies with latitude. Lower overhead O_3 inventories allow more UV into the lower stratosphere and upper troposphere, where enhanced photolysis of O_2 (*11*) increases O_3 by as much as +1.3%. The stratosphere-to-troposphere flux of O_3 [~500 Tg/year in this simulation (*12*, *13*)] increases by +0.9%, caused by O_3 increases in the mid-latitude lower stratosphere. The O_3 column near the surface is reduced by –0.45%, and thus reductions in lower tropospheric O_3 concentrations of about –0.2% are driven by increased UV and more rapid photochemical O_3 loss under moist conditions [$O(^1D) + H_2O$, $HO_2 + O_3$]. The global burden of CH_4 is decreased by –0.65% because of greater tropospheric OH abundances, caused by enhanced UV from the smaller O_3 column. Like N_2O, the relative perturbation of CH_4 declines further to –1.5% by 50 km because of the enhanced UV and loss in the middle stratosphere.

The use of chemical modes to deconstruct such perturbations allows for better understanding and predictions. Here we go beyond a one-dimensional (1D) representation of the N_2O chemical modes (*14*) by following the perturbations into 3D tropospheric chemistry. A relatively large reduction in CH_4 concentration (–3.6 ppb) is tied to an increase in N_2O (+10 ppb) that decays with a 108-year time scale. Thus, N_2O's climate impact through radiative forcing is diminished: (i) –8.4% because the decay of a pulse is faster than the e-fold of the steady-state lifetime used previously (*15*), and (ii) a further –4.5% to account for the decrease in the concentration of CH_4. For CH_4, the chemical feedbacks are opposite, lengthening the time scale of perturbations and increasing the greenhouse impact by about +40% (*16*–*18*).

Using the mode 1 coupling across species, one can readily compute that the N_2O concentration increase since preindustrial times, from 270 to 320 ppb, has caused a 2–Dobson unit (DU) (0.7%) decrease in total O_3 abundance, as compared with the 3.5% decrease since 1980 that is attributable primarily to halocarbons (*19*). The corresponding mode 1 offset in CH_4 since preindustrial times, –18 ppb, is small relative to the overall CH_4 concentration increase of 1000 ppb.

The agreed-on atmospheric residence time for CH_4 used to weight emissions in international treaties is based on the mode 2 time scale, currently estimated as 12 years (*20*). Our derived mode 2 time scale of 12.5 years is well within the uncertainty, but the ratio of residence to budget lifetime in our model is 1.6, at the upper end of the model range in that assessment. Our model thus predicts much stronger chemical feedbacks from CH_4 perturbations. The increase in global tropospheric O_3 per unit of increase in CH_4 is part of the mode 2 pattern calculated here, and the ratio in more traditional units, 3.1 DU per ppm, is similar to other model results [for example, 3.7 for (*2*) and 2.4 for (*1*)]. The CO-CH_4 coupling here, 7.4 Tg of CH_4 generated from 100 Tg of CO, is consistent with the indirect global warming potential of CO emissions (*18*).

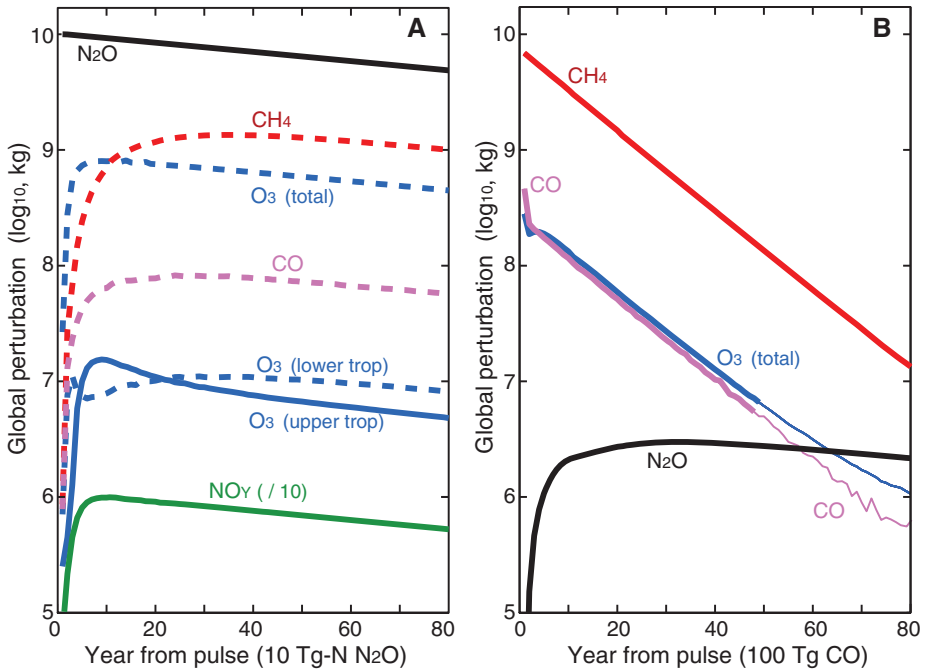

Fig. 1. Decay of atmospheric chemical perturbations caused by an initial pulse of (**A**) 10 Tg of N from N_2O and (**B**) 100 Tg of CO (1 Tg = 10^9 kg). Perturbations represent the total atmospheric burden of key species. Positive perturbations are indicated by solid lines; negative ones by dashed lines. The asymptotic behavior in (A) is chemical mode 1 with a decay time of 108 years. (B) shows both mode 2 (12.5 years) and mode 1 (N_2O only) decays. Values are plotted every 1 January, beginning 1 year after the initial pulse. The thin extension lines in (B) for O_3 (total) and CO indicate difficulties in separating the modes in both control C1 and perturbation C3.

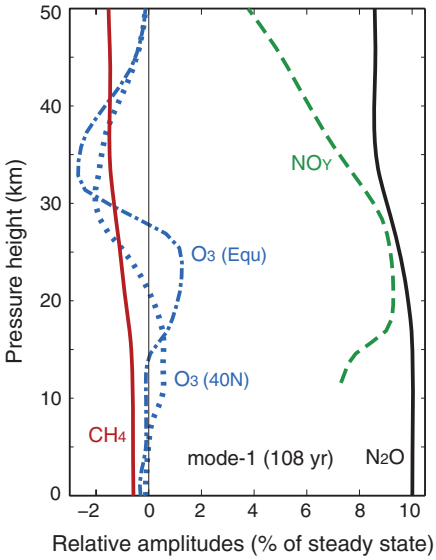

Fig. 2. Altitude profiles of the pattern of key species in mode 1 on 1 January. For N_2O, NOy, and CH_4, each profile is a global mean, but for O_3 the profiles are sampled at the equator and 40°N latitude. The amplitudes are shown as relative to the steady-state profiles and are scaled to 10% in N_2O at the surface.

Table 2. Chemical modes and amplitudes excited by pulses of N_2O, CO, and CH_4. The modes are identified with perturbation minus control (P − C) simulations. Amplitudes (*A*) are in globally integrated teragrams of N for N_2O and NOy and in teragrams for other species. The amplitudes of these modes are characterized by the amounts of N_2O (mode 1) and CH_4 (mode 2), shown in bold. Relatively small amplitudes are not shown (–).

P − C	Initial pulse	Mode (time)	*A* N_2O	*A* NOy	*A* CH_4	*A* O_3	*A* trop O_3
C2 − C1	10 Tg of N from N_2O	1 (108.4 years)	**+10.2**	+0.011	–2.1	–0.93	–0.01
		2 (12.5 years)	–0.002	–	**+2.8**	+0.11	0.03
C3 − C1	100 Tg of CO	1 (108.4 years)	**+0.0045**	–	–	–	–
		2 (12.5 years)	–0.005	–0.00003	**+7.4**	+0.30	+0.09
C4 − C1	10 Tg of CH_4	1 (108.4 years)	**+0.006**	–	–	–	–
		2 (12.5 years)	–0.007	-0.00004	**+9.85**	+0.40	+0.12

This N_2O-CH_4 coupling will shift with climate change over the 21st century. For example, the upper stratosphere cools as CO_2 increases, and this temperature change alters the N_2O-NOy-O_3 chemistry, reducing the impact of N_2O on O_3 (*21*). The importance of N_2O as an ozone-depleting substance (*22*) will thus be reduced, weakening the coupling described here but still maintaining the negative greenhouse feedback effect of CH_4 on N_2O emissions.

References and Notes

1. A. M. Fiore, J. J. West, L. W. Horowitz, V. Naik, M. D. Schwarzkopf, *J. Geophys. Res.* **113**, D08307 (2008).
2. M. Prather *et al.*, in *Climate Change 2001: The Scientific Basis. Third Assessment Report of the Intergovernmental Panel on Climate Change*, J. T. Houghton *et al.*, Eds. (Cambridge Univ. Press, Cambridge, 2001), pp. 239–287.
3. M. B. McElroy, J. C. McConnell, *J. Atmos. Sci.* **28**, 1095 (1971).
4. World Meteorological Organization (WMO), *Atmospheric Ozone 1985: Assessment of Our Understanding of the Processes Controlling Its Present Distribution and Change*, R. T. Watson *et al.*, Eds. (Global Ozone Research and Monitoring Project Report No. 16, WMO, Geneva, 1985).
5. J. Hsu, M. J. Prather, *Geophys. Res. Lett.* **37**, L07805 (2010).
6. Q. Tang, M. J. Prather, *Atmos. Chem. Phys.* **10**, 9681 (2010).
7. Materials and methods are available as supporting material on *Science* Online.
8. D. S. Stevenson *et al.*, *J. Geophys. Res.* **111**, D08301 (2006).
9. O. Wild, M. J. Prather, *J. Geophys. Res.* **105**, 24647 (2000).
10. R. G. Derwent, W. J. Collins, C. E. Johnson, D. S. Stevenson, *Clim. Change* **49**, 463 (2001).
11. M. J. Prather, *Geophys. Res. Lett.* **36**, L03811 (2009).
12. J. Hsu, M. J. Prather, O. Wild, *J. Geophys. Res.* **110**, D19305 (2005).
13. J. Hsu, M. J. Prather, *J. Geophys. Res.* **114**, D06102 (2009).
14. M. J. Prather, *Science* **279**, 1339 (1998).
15. D. L. Albritton, R. G. Derwent, I. S. A. Isaksen, M. Lal, D. J. Wuebbles, in *Climate Change 1994, Intergovernmental Panel on Climate Change*, J. T. Houghton *et al.*, Eds. (Cambridge Univ. Press, Cambridge, 1995), pp. 204–231.
16. M. J. Prather, *Geophys. Res. Lett.* **21**, 801 (1994).
17. M. Prather *et al.*, in *Climate Change 1994, Intergovernmental Panel on Climate Change*, J. T. Houghton *et al.*, Eds. (Cambridge Univ. Press, Cambridge, 1995), pp. 73–126.
18. P. Forster *et al.*, in *Climate Change 2007: The Physical Science Basis. Fourth Assessment Report of the Intergovernmental Panel on Climate Change*, S. Solomon *et al.*, Eds. (Cambridge Univ. Press, Cambridge, 2007), pp. 129–234.
19. WMO, *Scientific Assessment of Ozone Depletion: 2006*, C. A. Ennis, Ed. (WMO, Geneva, 2006).
20. K. L. Denman *et al.*, in *Climate Change 2007: The Physical Science Basis. Fourth Assessment Report of the Intergovernmental Panel on Climate Change*, S. Solomon *et al.*, Eds. (Cambridge Univ. Press, Cambridge, 2007), pp. 499–587.
21. J. E. Rosenfield, A. R. Douglass, *Geophys. Res. Lett.* **25**, 4381 (1998).
22. A. R. Ravishankara, J. S. Daniel, R. W. Portmann, *Science* **326**, 123 (2009).

23. This research was supported by NSF's Atmospheric Chemistry program (grant ATM-0550234) and NASA's Modeling, Analysis, and Prediction/Global Modeling Initiative program (grants NNG06GB84G and NNX09AJ47G).

Supporting Online Material

www.sciencemag.org/cgi/content/full/330/6006/952/DC1
Methods
References

9 August 2010; accepted 8 October 2010
10.1126/science.1196285

Fossil Evidence for Evolution of the Shape and Color of Penguin Feathers

Julia A. Clarke,[1]* Daniel T. Ksepka,[2,3] Rodolfo Salas-Gismondi,[4] Ali J. Altamirano,[4] Matthew D. Shawkey,[5] Liliana D'Alba,[5] Jakob Vinther,[6] Thomas J. DeVries,[7] Patrice Baby[8,9]

Penguin feathers are highly modified in form and function, but there have been no fossils to inform their evolution. A giant penguin with feathers was recovered from the late Eocene (~36 million years ago) of Peru. The fossil reveals that key feathering features, including undifferentiated primary wing feathers and broad body contour feather shafts, evolved early in the penguin lineage. Analyses of fossilized color-imparting melanosomes reveal that their dimensions were similar to those of non-penguin avian taxa and that the feathering may have been predominantly gray and reddish-brown. In contrast, the dark black-brown color of extant penguin feathers is generated by large, ellipsoidal melanosomes previously unknown for birds. The nanostructure of penguin feathers was thus modified after earlier macrostructural modifications of feather shape linked to aquatic flight.

During wing-propelled diving, penguins generate propulsive forces in a fluid environment ~800 times more dense and ~70 times more viscous than air (*1*). Recent fossil discoveries have yielded information on the sequence of early osteological changes in penguins accompanying the evolution of aquatic flight (*2*–*5*), but these specimens have not included feathers. Living penguin melanosome morphologies have not been described, although the melanin they contain is generally known to provide both color and wear-resistance to bird feathers (*6*–*8*). Here, we describe a giant fossil penguin with feathers recording preserved melanosome morphologies (*9*) and discuss the pattern and timing of major events in the evolution of penguin integument.

Systematic paleontology: Aves Linnaeus 1758 *sensu* Gauthier 1986. Sphenisciformes Sharpe 1891 *sensu* Clarke *et al*. 2003. *Inkayacu paracasensis* new gen. and sp. **Etymology:** *Inkayacu*—the Quechua, "Inka" for emperor and "yacu" for water; *paracasensis* for the Reserva Nacional de Paracas, Peru, the type locality. **Holotype**: MUSM 1444, a nearly complete skeleton with wing feathering, body contour feathers, and pedal scales (Figs. 1 to 3) (*10*). **Locality and horizon:** Upper Eocene of Yumaque Point, Paracas Reserve, Peru (*10*). **Diagnosis:** *Inkayacu paracasensis* is diagnosed by the following combination of characters (autapomorphies within Sphenisciformes demarcated by an asterisk): paired grooves meeting at midline on dorsal surface of premaxilla* (Fig. 1, GR), articular surfaces of otic and squamosal head of quadrate contacting one another,* furcula with blade-like hypocleidium,* conspicuous n. coracobrachialis sulcus developed on the humerus (Fig. 1, CNS), femur with widened and sharply distally tapering medial condyle* and tab-like process projecting from posterior intramuscular ridge at midshaft* (Fig. 1, MC and T), and weak proximal projection of cnemial crests of tibiotarsus (Fig. 1, CNE). See (*10*) for additional diagnosis, figures, and description.

[1]Department of Geological Sciences, University of Texas at Austin, Austin, TX 78712, USA. [2]Department of Marine, Earth, and Atmospheric Sciences, North Carolina State University, Raleigh, NC 27695–8208, USA. [3]Department of Paleontology, North Carolina Museum of Natural Sciences, Raleigh, NC 27601–1029, USA. [4]Departamento de Paleontología de Vertebrados, Museo de Historia Natural–Universidad Nacional Mayor de San Marcos (UNMSM), Lima 14, Perú. [5]Integrated Bioscience Program, University of Akron, Akron, OH 44325, USA. [6]Department of Geology and Geophysics, Yale University, New Haven, CT 06511, USA. [7]Burke Museum of Natural History and Culture, University of Washington, Seattle, WA 98195, USA. [8]Laboratoire des Mécanismes et Transferts en Géologie, Institut de Recherche pour de Développement, 14 Avenue Edouard Belin, F-31400 Toulouse, France. [9]Université de Toulouse, F-31400 Toulouse, France.

*To whom correspondence should be addressed: julia_clarke@jsg.utexas.edu